

A Generalized Parallel Transmission Line Iteration for Finite Element Analysis of Permanent Magnet Axisymmetrical Actuator

Wenyang Yang¹, Fei Peng¹, Venkata Dinavahi², and Guofu Zhai¹

¹School of Electrical Engineering and Automation, Harbin Institute of Technology, Harbin 150001 China

²Department of Electrical and Computer Engineering, University of Alberta, Edmonton, AB T6G 2V4, Canada

At present, finite element method (FEM) is still the mainstream tool in a range of complex science and engineering applications, including the analysis of structures, heat, fluid, and electromagnetics. However, FEM becomes computationally very intensive when the number of physics equations grows and the mesh is refined. In this paper, we investigated the parallel computing techniques in the nonlinear magnetostatic field solution of an axisymmetrical actuator with permanent magnet by proposing a generalized black-box transmission line method (BB-TLM). A novel black-box circuit model was built to represent complex FEM element data. By means of the transmission line model, each element is isolated and then a series of parallel procedures is considered during the solution stages. The magnetic field distribution and magnetic force of the studied actuator are calculated by the proposed method and the simulation results are compared with COMSOL. Compared with the conventional N-R method, the generalized BB-TLM algorithm greatly reduces the computation time.

Index Terms—Axisymmetric magnetostatic analysis, electromagnetic device, finite element method (FEM), multi-thread, nonlinear magnetostatic, parallel processing, TLM.

I. INTRODUCTION

ELECTROMAGNETIC devices have been widely used in industrial applications. The static and dynamic analysis of those devices with nonlinear materials is the basic problem in product design and manufacture. From the traditional magnetic circuit method to recent numerical computation method, finite element method (FEM) plays an important role in present-day engineering analysis of the complex system simulation. Nevertheless, it is generally acknowledged that FEM is a time-consuming and computationally intensive process for most problems, particularly with the increase of FEM mesh elements and model complexity. It is no doubt that performing FEM computation efficiently is a vital issue to research.

Time cost in finite element computation appears in various stages of the solution. One of the improvements in computational efficiency is focused on the mesh generation. In [1]–[3], a parallel 3-D mesh refinement based on dynamic load balancing algorithm was proposed. The method allows for a relatively detailed description of the system and revealed key performance characteristics. In the aspect of performing the assembly of the system matrix efficiently, Markall *et al.* [4] implemented the parallel assembly independently on a multi-core CPU and many-core GPU by partitioning the mesh into several regions. Similarly, multiple strategies in assembling and solving were proposed in [5] for low-order and high-order elements. In addition, in [6]–[8], a matrix-free FEM implemented on GPU was proposed which can be used in

a wide range of situations. In this method, no assembly is needed. However, an iterative solver must be used.

Another performance bottleneck in most finite element applications is the nonlinear iteration solution stage. To improve the computation speed, the related works on serial algorithms, including the direct iteration method, Newton–Raphson, and so on, were implemented and the relaxation method was used to reduce the iteration times [9], [10]. With the advent of multi-core computing resources, many studies started to focus on the parallelism of the solution method, for example, Hoole and Mahinthakumar [11] proposed a parallelizing technique of iterative process when FEM was used to calculate electromagnetic problems and pointed out that the pre- and post-processing of FEM should also be considered for parallelization. The parallel boundary element method and serial FEM were combined in [12] and were used in the GMRES iterations. The method not only sped up the computation but also overcame the limited storage of a single computer. An evaluation of the numerical simulation of electrical machines by means of a hybrid parallelization of the FEM-package iMOOSE was given using the standardized paradigms OpenMP and Message Passing Interface in [13]. The evaluation showed that the solution process of the system of equations limited the possible speed-up owing to increasing number of required iterations with increasing number of used cores. Amestoy *et al.* [14] tested significant improvements of parallel sparse direct solver MULTifrontal Massively Parallel sparse direct Solver in 3-D numerical simulation of induction heating industrial applications. Results showed a remarkable reduction of both memory usage and number of performed operations. Furthermore, both tree and node parallelisms were exploited to reduce the solution time.

Like the Newton–Raphson iteration, the TLM iteration method can be used to solve nonlinear systems. In the

Manuscript received July 8, 2018; revised September 19, 2018 and November 11, 2018; accepted December 4, 2018. Date of publication January 4, 2019; date of current version February 15, 2019. This work was supported by the National Natural Science Foundation of China under Grant 51507033. Corresponding author: W. Yang (e-mail: yangwy@hit.edu.cn).

Color versions of one or more of the figures in this paper are available online at <http://ieeexplore.ieee.org>.

Digital Object Identifier 10.1109/TMAG.2018.2885966

beginning, TLM was applied in the problem of electrical system and circuit network [15]–[17]. Then, it was exploited as a new way to solve the nonlinear magnetostatic problem along with the FEM method [18]. Because the TLM method has some advantages in computation efficiency, some researchers started to apply it in the nonlinear calculation of finite element. In [19]–[21], the eddy-current problems in induction machines were studied and combined it with domain decomposition technique. Asghari and Dinavahi [22], [23] also studied the transient simulation of induction machines using an improved TLM method. In recent works, a novel equivalent finite-element network's circuit model was proposed to apply TLM into the solution of an axisymmetrical magnetostatic problem [24]. The key point to the application of TLM in FEM is how to transfer the mesh network to an equivalent circuit system. However, it is easy to conclude that the applications of TLM are limited to the first order triangle element and current approaches are unsuitable for complex FEM elements, such as quadrilateral shape element and tetrahedron element.

To further improve the practicality of TLM, in this paper, we propose a novel black-box transmission line method (BB-TLM) method to speed up the nonlinear FEM solution for an axisymmetrical actuator with permanent magnet. The proposed black-box model not only reduces the difficulties in building equivalent circuit of FEM matrices but also can easily solve the nonlinear relationship in each nonlinear FEM element using Newton–Raphson method. The TLM method can be applied into various FEM elements using our models, such as triangular shape element and quadrilateral shape element. In addition, because each nonlinear element is disconnected from each other, this method can also be parallelized with the help of parallel programming techniques. By comparison with simulation results, comparisons show that the proposed method could significantly speed up the computation with acceptable solution accuracy.

The rest of this paper is organized as follows. Section II describes the FEM in axisymmetrical magnetostatic field. Section III introduces the proposed black-box TLM iterative method in nonlinear FEM solution. Section IV provides the simulation results of a typical contactor with permanent magnet actuator and gives the comparison of different methods. Finally, Section V presents conclusions and future prospects.

II. FINITE ELEMENT METHOD FOR MAGNETOSTATIC FIELD OF AXISYMMETRICAL ACTUATOR

To obtain the distribution graph of magnetic field, the FEM is employed in the solution of actuator's magnetostatic problem. In this section, the 2-D axisymmetrical case is studied, as shown in Fig. 1.

A. Governing Equation

In the actuator, the magnetostatic field obeys the following equation:

$$\nabla \times \frac{1}{\mu} \nabla \times \mathbf{A} = \mathbf{J} \quad (1)$$

where μ is the permeability of material, \mathbf{A} is the magnetic field potential vector, and \mathbf{J} is the current density.

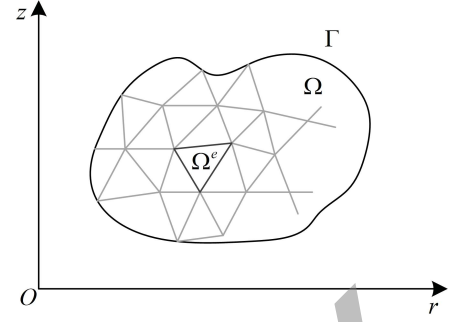


Fig. 1. Discretization of solution domain Ω .

In the cylindrical coordinate system (r, z, ϕ) , for the axisymmetrical structure, we have

$$\begin{cases} A_r = A_z = 0, & A_\phi = A \\ J_r = J_z = 0, & J_\phi = J. \end{cases} \quad (2)$$

Then, (1) is simplified as

$$\frac{\partial}{\partial z} \left(\frac{1}{\mu'} \frac{\partial A'}{\partial z} \right) + \frac{\partial}{\partial r} \left(\frac{1}{\mu'} \frac{\partial A'}{\partial r} \right) = -J \quad (3)$$

where $\mu' = r\mu$ and $A' = rA$.

B. Boundary Conditions

Two types of boundary conditions are imposed in the solution.

1) The magnetic potential A is zero in the infinite space, assuming that the outer boundary is at infinity, therefore, we have the first type boundary condition

$$\Gamma_1 : A' = 0. \quad (4)$$

2) In addition, the z -axis is also applied with the second-type boundary condition

$$\Gamma_2 : \frac{\partial A'}{\partial \mathbf{n}} = 0. \quad (5)$$

C. Galerkin's Method

To convert the above-mentioned differential equation into a discrete problem, Galerkin's method of weighted residuals is usually used to calculate the global stiffness matrix in the finite element [25].

For a single discretized element Ω^e in domain Ω in Fig. 1, the unknown quantity A' is interpolated using a set of Lagrange polynomials, that is,

$$A' = \sum_{j=1}^n A_j^{e'} N_j \quad (6)$$

where $A_j^{e'}$ is the magnetic potential at each node of element Ω^e , N_j is the shape function, and n is the number of local nodes per element.

Applying Galerkin's method, (3) can be discretized as

$$\begin{aligned} \iint_{\Omega^e} \frac{1}{\mu'} \left[\frac{\partial N_i}{\partial r} \left(\sum_{j=1}^n A_j^{e'} \frac{\partial N_j}{\partial r} \right) + \frac{\partial N_i}{\partial z} \left(\sum_{j=1}^n A_j^{e'} \frac{\partial N_j}{\partial z} \right) \right] d\Omega^e \\ = \iint_{\Omega^e} J N_i d\Omega^e \quad (i = 1, 2, \dots, n) \end{aligned} \quad (7)$$

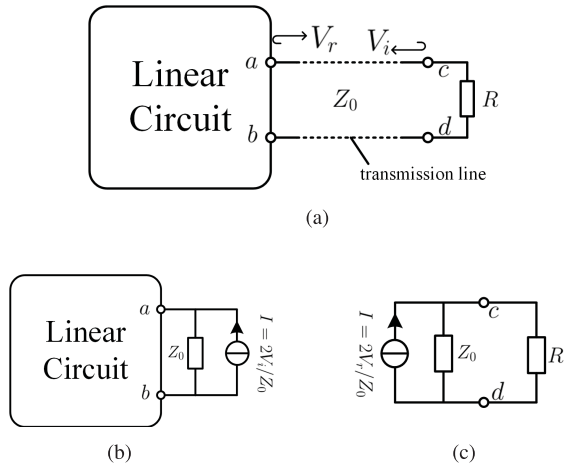


Fig. 2. Transmission line in circuit network. (a) Nonlinear resistance with lossless transmission line. (b) Equivalent circuit during incidence process. (c) Equivalent circuit during reflection process.

in domain Ω^e which can be rewritten as matrix form

$$\begin{bmatrix} K_{11}^e & K_{12}^e & \cdots & K_{1n}^e \\ K_{21}^e & K_{22}^e & \cdots & K_{2n}^e \\ \vdots & \vdots & \ddots & \vdots \\ K_{n1}^e & K_{n2}^e & \cdots & K_{nn}^e \end{bmatrix} \begin{bmatrix} A_1^{e'} \\ A_2^{e'} \\ \vdots \\ A_n^{e'} \end{bmatrix} = \begin{bmatrix} b_1^e \\ b_2^e \\ \vdots \\ b_n^e \end{bmatrix} \quad (8)$$

or simply expressed as a nonlinear matrix equation about μ' , that is,

$$K^e A^{e'} = b^e \quad (9)$$

where

$$\begin{cases} K_{ij}^e = \iint_{\Omega^e} \frac{1}{\mu'} \left[\frac{\partial N_i}{\partial r} \frac{\partial N_j}{\partial r} + \frac{\partial N_i}{\partial z} \frac{\partial N_j}{\partial z} \right] d\Omega^e \\ b_i^e = \iint_{\Omega^e} J N_i d\Omega^e \quad (i, j = 1, 2, \dots, n). \end{cases} \quad (10)$$

By assembling the element coefficient matrix K^e and right-side matrix b^e in each element, we obtain the nonlinear global matrix system

$$K A' = b \quad (11)$$

where K is the global coefficient matrix, A' is the unknown magnetic potential, and b is the global right-hand side matrix.

III. BLACK-BOX TLM METHOD IN FEM

Equation (11) is usually solved by Newton–Raphson iteration. In addition, the TLM method can also be used to solve the nonlinear systems which originated from Branin’s method [26]. In recent years, TLM was successfully used in the parallel computation of FEM [27], [28]. However, there still exist some challenges in the application.

A. Basic TLM Iteration Process in Circuit

The TLM iteration basically includes two stages: incidence and reflection. As shown in Fig. 2, assuming that the voltage signal is propagating along the lossless transmission line between a and c , at a moment, when the incidence voltage

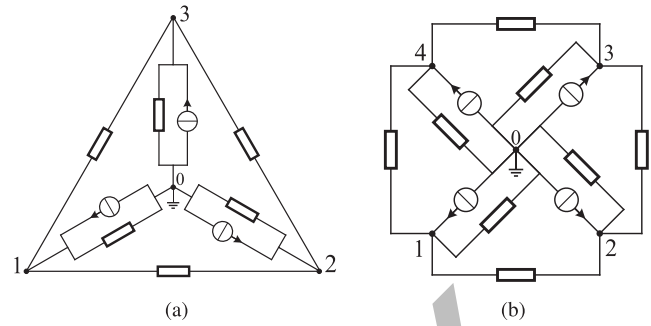


Fig. 3. Nonlinear equivalent circuits obtained by conventional TLM method. (a) Nonlinear equivalent circuit of triangular finite element when $n = 3$. (b) Nonlinear equivalent circuit of quadrilateral shape finite element when $n = 4$.

V_i travels from c to a , if an observer stands at a , the Norton equivalent circuit is shown in Fig. 2(b). At next moment, when the voltage signal arrives at a and reflects to c , the reflection voltage V_r can be obtained by

$$V_r = V_{ab} - V_i \quad (12)$$

where V_{ab} is the voltage difference between a and b . Then, if an observer stands at c , the equivalent circuit is shown in Fig. 2(c). When the voltage signal arrives at c and reflects to a , the incidence voltage of next time is given as

$$V_i = V_{cd} - V_r \quad (13)$$

where V_{cd} is the voltage difference between c and d . This is one iteration process of TLM and voltage signals will not stop reflecting until $V_{ab} = V_{cd}$. The transmission lines successfully split the circuit in Fig. 2(a) into circuits in Fig. 2(b) and (c). The linear part and nonlinear part R are iterated in different stages.

B. Drawbacks of Original TLM Method

The idea of building an equivalent circuit is based on the fact that FEM’s global coefficient matrix K is obtained by assembling all elements’ unit matrices together and K is also a positive definite and symmetric matrix. Therefore, it is possible to model each element matrix as a small circuit block. Then, we can group all these small pieces together as an equivalent circuit network. Thus, the FEM problem (11) can be solved in a circuit manner.

In original TLM iteration, the right-hand side matrix b^e is modeled as current sources flowing into the nodes and the coefficient matrix K^e is treated as nodal admittance matrix in circuit, where K_{ii}^e ($i = 1, 2, \dots, n$) is the self-admittance of node i and K_{ij}^e ($i, j = 1, 2, \dots, n; i \neq j$) is the mutual admittance between nodes i and j . This kind of method especially works for one order triangular element which is used by most researchers. However, it still faces challenges when it is applied to different elements or shape functions.

Fig. 3 illustrates the general nonlinear equivalent circuits when the number of element nodes is $n = 3$ and $n = 4$, respectively. Each element contains $2n$ nonlinear components and n current sources. Consequently, with the increase of n

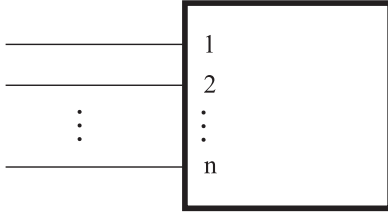


Fig. 4. Black-box model of an n -nodes FEM element.

and the number of mesh elements, the size of equivalent circuit also increases and memory consumption will be greater.

Besides the complex internal circuit, the conventional TLM method also has difficulty dealing with the nonlinear relationship existing in different components of single element during the reflection process. Assuming that R_i^e and Y_i^e ($i = 1, 2, \dots, 2n$) are the i th nonlinear component's impedance and admittance derived from FEM matrix, respectively, we know it is a nonlinear function of unknown magnetic potential $A_i^{e'}$ ($i = 1, 2, \dots, n$) of each node, that is,

$$Y_i^e = 1/R_i^e = f_i(A_1^e, A_2^e, \dots, A_n^e). \quad (14)$$

When the signals reflect back to the element, those $2n$ small circuits in the element Ω^e need to be solved simultaneously, corresponding to the circuit in Fig. 2(c). It is a set of $2n$ dependent nonlinear equations

$$\begin{cases} I_1 = V_1 \cdot Y_1^e(A_1^e, A_2^e, \dots, A_n^e) \\ I_2 = V_2 \cdot Y_2^e(A_1^e, A_2^e, \dots, A_n^e) \\ \vdots \\ I_{2n} = V_{2n} \cdot Y_{2n}^e(A_1^e, A_2^e, \dots, A_n^e). \end{cases} \quad (15)$$

It should be noted that the $2n$ small circuits are not all connected with each other and there does not exist a common ground. Equation (15) is difficult to be solved considering that there are $2n + n$ unknown variables (V_1, \dots, V_{2n} and A_1^e, \dots, A_n^e) and the number of equations increases with the number of FEM's element nodes increases.

C. New Black-Box Equivalent Circuit Model and Iteration Process in FEM

To better solve the two problems described earlier, we employ a new black-box model in Fig. 4 to encapsulate and represent the circuit information inside each element in Fig. 3. This new complex circuit component has nothing outside but n pins which correspond to n nodes of each element. In this case, the black-box's internal nonlinear information is simply expressed by matrix K^e in (9). Thus, the complicated equivalent circuit modeling process in Fig. 3 can be omitted. This is the first advantage of the black-box model.

The new TLM iteration still includes two stages: incidence and reflection. Fig. 5 presents the novel equivalent circuit network of FEM problems and its iteration processes. In Fig. 5(a), those elements in linear regions of FEM are modeled as a linear circuit network whose admittance matrix is given as FEM's coefficient matrix. Those nonlinear elements are

built as black-box circuit models connected with each other through FEM nodes. To take advantage of the TLM method, n transmission lines are inserted into the black-box's output pins and signals travel back and forth. It should be noted that transmission line in Fig. 2(a) has two wires: ac and bd , whereas in our model in Fig. 5(a), the wire cd is connected with the ground. Thus, the equivalent circuit of the incidence process is illustrated as Fig. 5(b). This circuit can be solved by

$$(Y_{\text{linear}} + Y_{\text{TL}})A' = b + 2V_i Y_{\text{TL}} \quad (16)$$

where Y_{linear} is the admittance matrix of the linear network, Y_{TL} is the admittance matrix including all the transmission lines' admittances, and $2V_i Y_{\text{TL}}$ is the fictitious current sources. The reflection voltage V_r is updated by

$$V_r = A' - V_i. \quad (17)$$

When signals travel back to the elements, all the nonlinear elements are disconnected with each other because of transmission lines, and the equivalent circuit is shown in Fig. 5(c). The nonlinear system equation is simply written as

$$(K^e + Y_{\text{TL}}^e)A^{e'} = 2V_r^e Y_{\text{TL}}^e \quad (18)$$

which can be solved by the Newton iteration with a convergence error of δ which can also be called inner iteration error of BB-TLM. The k th Newton iteration form of nonlinear (18) is given as

$$(J_k^e + Y_{\text{TL}}^e)A_{k+1}^{e'} = 2V_r^e Y_{\text{TL}}^e + (J_k^e - K_k^e)A_k^{e'} \quad (19)$$

where K_k^e is the admittance matrix of the nonlinear element in k th Newton iteration, $2V_r^e Y_{\text{TL}}^e$ is the fictitious current sources, and J_k^e is the Jacobian matrix in k th Newton iteration which is calculated by

$$J^e = \begin{bmatrix} \frac{\partial f_1}{\partial A_1^e} & \frac{\partial f_1}{\partial A_2^e} & \cdots & \frac{\partial f_1}{\partial A_n^e} \\ \frac{\partial f_2}{\partial A_1^e} & \frac{\partial f_2}{\partial A_2^e} & \cdots & \frac{\partial f_2}{\partial A_n^e} \\ \vdots & \vdots & \ddots & \vdots \\ \frac{\partial f_n}{\partial A_1^e} & \frac{\partial f_n}{\partial A_2^e} & \cdots & \frac{\partial f_n}{\partial A_n^e} \end{bmatrix} \quad (20)$$

and

$$\begin{bmatrix} f_1 \\ f_2 \\ \vdots \\ f_n \end{bmatrix} = \begin{bmatrix} K_{11}^e & K_{12}^e & \cdots & K_{1n}^e \\ K_{21}^e & K_{22}^e & \cdots & K_{2n}^e \\ \vdots & \vdots & \ddots & \vdots \\ K_{n1}^e & K_{n2}^e & \cdots & K_{nn}^e \end{bmatrix} \begin{bmatrix} A_1^{e'} \\ A_2^{e'} \\ \vdots \\ A_n^{e'} \end{bmatrix}. \quad (21)$$

Equation (18) not only has fewer equations than (15) but also it can be implemented using the same Jacobian matrix in conventional Newton-Raphson method. This is the second advantage of the black-box model. Then, the incidence voltage V_i in each element is updated by

$$V_i^e = A^{e'} - V_r^e. \quad (22)$$

Similarly, the voltage signals will not stop reflecting until the solution converges.

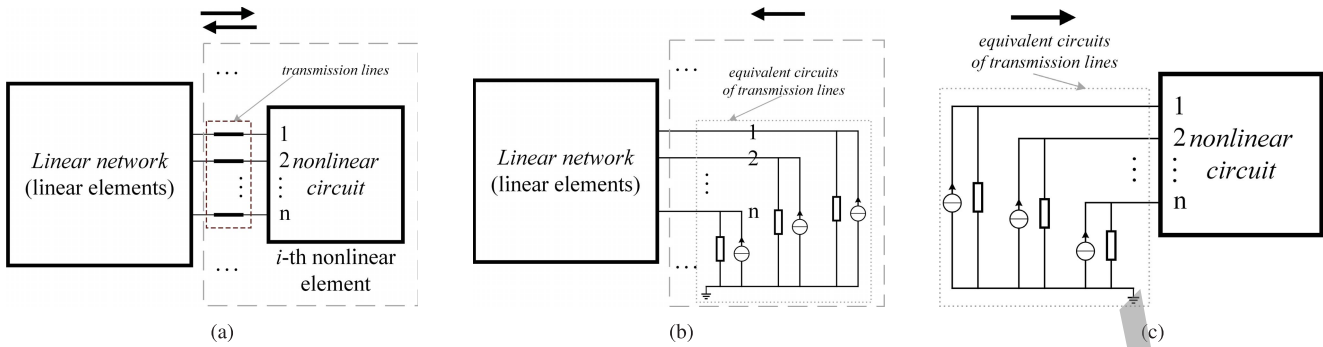


Fig. 5. New TLM equivalent circuit model in FEM and its iteration process. (a) New equivalent circuit in FEM with transmission lines. (b) Linear equivalent circuit network when voltage signals travel toward linear network of FEM. (c) Nonlinear equivalent circuit of FEM's single element when voltage signals travel back.

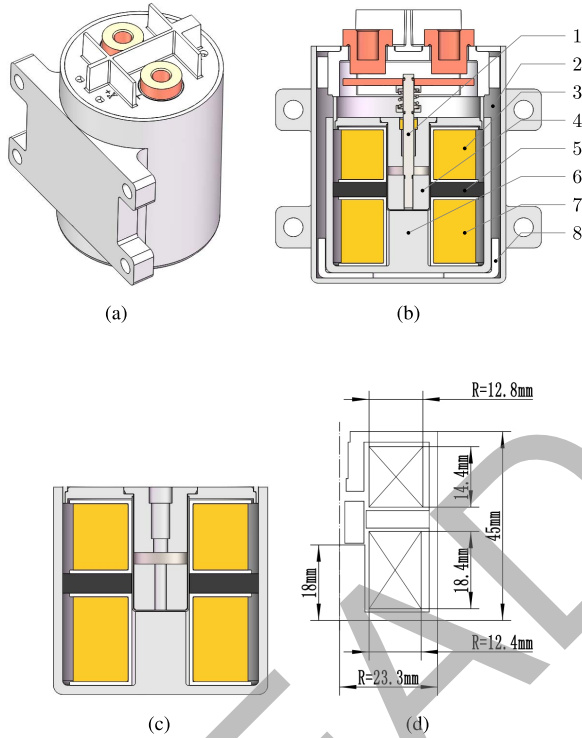


Fig. 6. Structure of the axisymmetrical contactor with permanent magnet actuator (1: nonmagnetic shaft; 2: metal cover; 3: top coil; 4: armature; 5: permanent magnet; 6: iron core; 7: bottom coil; and 8: plastic cover). (a) Appearance of the contactor. (b) View of cross section. (c) Simplified model. (d) Dimensions of one half actuator model.

IV. CASE STUDY

A. Description of an Axisymmetrical Contactor With Permanent Magnet Actuator

The contactor with permanent magnet actuator is a novel electromagnetic device, which combines solenoid with permanent magnet achieving the function of operation. It is a bistable equipment and works very similar to the traditional contactor. It still operates by the principle of electromagnetics, however, its status is retained after power off with the help of permanent magnet. Therefore, this kind of contactor avoids certain drawbacks of traditional electromagnetic contactor, and it can work with high reliability, small power consumption, and ability of anti-vibration.

As shown in Fig. 6, it is a typical dc axisymmetrical contactor prototype with permanent magnet actuator which has

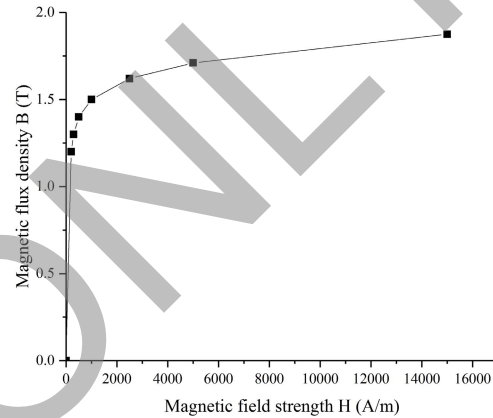


Fig. 7. $B-H$ curve of material DT4E.

a weight of 0.45 kg and a size of 75 mm \times 55 mm \times 79.1 mm. It mainly consists of metal cover, plastic cover, sleeve, iron core (material: DT4E), permanent magnet (NdFeB), coil, armature, non-magnetic shaft (stainless steels), and so on. The magnetization direction of permanent magnet is along the horizontal direction. The coercivity H_c of NdFeB is 88310 A/m and its remanence B_r is 1.21 T. The $B-H$ curve of material DT4E is shown in Fig. 7.

B. Solution Process of the Magnetostatic Field

To verify the accuracy, effectiveness, and flexibility of the proposed method, in this section, the actuator model is studied by both N-R and black-box TLM method. The flowchart of BB-TLM is shown in Fig. 8. At first, the allocation of memory, the setting of material properties and other procedures will be implemented before the iteration. Then, the admittance of the circuit network in Fig. 5(b) will be assembled and its lower-upper (LU) factorization will be done in advance since it remains unchanged during the whole iterative process. Finally, we run the BB-TLM iteration. When the voltage signals travel toward the nonlinear elements, because of the independence of each element, the N-R iteration in each element can be performed in single hardware computational core using parallel techniques. Then, voltage signals travel back toward the linear region where the solution of the circuit network can be obtained by forward and backward substitution

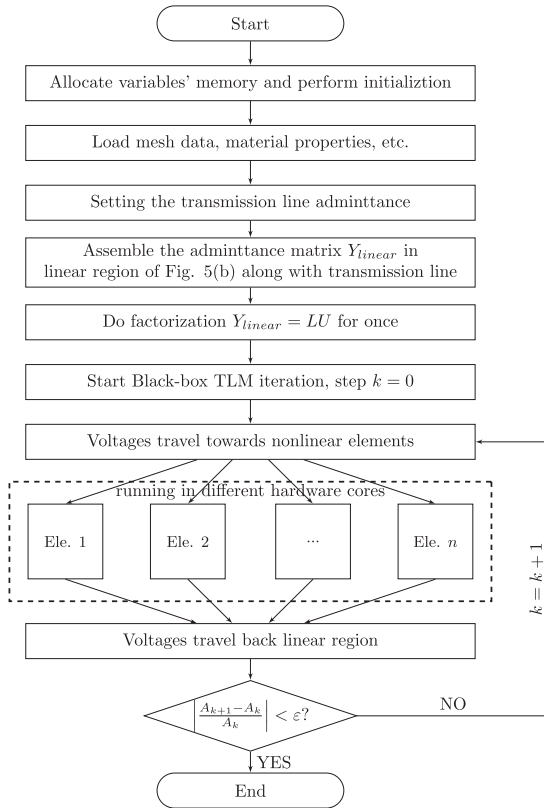


Fig. 8. Flowchart of the proposed black-box TLM method.

TABLE I
DIFFERENT COMPUTATIONAL MODELS

Cases	Mesh size	Nodes size	Nonlinear elements	Cases	Mesh size	Nodes size	Nonlinear elements
1	6690	3392	1706	6	6749	6910	843
2	10635	5371	2564	7	8685	8757	2415
3	19221	9691	4458	8	12226	12403	1565
4	26637	13404	6323	9	19246	19526	1031
5	46676	23515	10610	10	35928	36336	2451

of triangular matrices (L and U) for different right-hand side vectors. Those codes were run on a multi-core workstation which has two Intel Xeon Processors E5-2670 v3 (30M Cache, 2.30 GHz). To make it easier to simulate and analyze, in Fig. 6(c), some simplifications are applied to the model. Given the axisymmetric nature of actuator's structure, we use one-half of it for calculation. The FEM mesh models used are presented in Table I where cases 1–5 and 6–10 are triangular elements and quadrilateral shape elements of different mesh sizes, respectively.

C. Distribution of Magnetic Field

Fig. 9 shows the distribution of magnetic potential at different positions of the actuator computed by BB-TLM. It includes two kinds of operating positions: open and closed, and two modes of the coils. The coil working voltage is 28 V. From Fig. 9, we can further explore the variation of magnetic

TABLE II
COMPARISON OF COMPUTATIONAL ERRORS OF MAGNETIC POTENTIAL (Wb/m) AMONG COMSOL, N-R, AND BB-TLM

No.	r/mm	z/mm	COMSOL (Wb/m)	N-R (Wb/m)	err ₁ ¹	BB-TLM (Wb/m)	err ₂ ²
1	6.6	-1	2.71E-05	2.70E-05	0.32%	2.70E-05	0.35%
2	7.1	14	-1.25E-05	-1.24E-05	0.65%	-1.24E-05	0.94%
3	15.6	-3.9	4.25E-05	4.05E-05	4.71%	4.05E-05	4.69%
4	14.9	3.3	-2.47E-05	-2.41E-05	2.46%	-2.41E-05	2.39%
5	7.4	-10.8	3.16E-05	3.06E-05	3.15%	3.06E-05	3.17%
6	7.2	-3	2.01E-05	1.95E-05	2.60%	2.10E-05	4.93%
7	19.8	-1.2	3.96E-05	4.07E-05	2.77%	4.11E-05	3.79%
8	6	-8.5	2.26E-05	2.19E-05	3.00%	2.34E-05	3.45%
9	5.8	18.4	-2.75E-05	-2.77E-05	0.86%	-2.63E-05	4.11%
10	15.8	3	-3.63E-05	-3.50E-05	3.80%	-3.71E-05	2.15%

$${}^1err_1 = \left| \frac{N-R - COMSOL}{COMSOL} \right| \times 100\%$$

$${}^2err_2 = \left| \frac{BB-TLM - COMSOL}{COMSOL} \right| \times 100\%$$

strength with respect to the changes in structure and current sources. In Fig. 9(a) and (b), when the lower coil is working, the magnetic potential in the bottom region of actuator is increasing with the armature moving from closed position to open position. In Fig. 9(c) and (d), when the upper coil is working, the magnetic potential in the top region of actuator is increasing with the armature moving from open position to closed position. In every new position, a closed magnetic loop is formed which makes the attraction more stable.

To demonstrate the accuracy of the codes, Table II presents the relative computational error of N-R and BB-TLM compared with commercial FEM software COMSOL. Cases 1–5 are five random points selected from model case 5 in Table I, and cases 6–10 are five random points selected from model case 10 in Table I. The locations of the 10 points can be found in Fig. 9(b) and (c). Results show that the relative error is within 5% which is acceptable.

In addition, Table III illustrates the comparison of magnetic flux density values among COMSOL, N-R, and BB-TLM. Ten points are chosen randomly using the same method in Table II. Although the relative errors of Nos. 8 and 10 are the biggest, it turns out that most results of N-R and BB-TLM agree well with that of COMSOL. The N-R method also has obvious errors at those locations. Considering that the coordinates of Nos. 8 and 10 are close to the z-axis and the B values are very small, the calculation errors could be understandable. The comparisons of magnetic potential and magnetic flux density suggest BB-TLM can be applied to both triangular and quadrilateral shape elements with acceptable errors.

D. Comparison of Magnetic Forces

To further prove the accuracy of BB-TLM, the comparisons of magnetic forces exerted on the armature between BB-TLM and COMSOL are given in Fig. 10 where the magnetic forces are calculated at different positions of armature by the Coulomb virtual work method [29], [30]. The distance of open

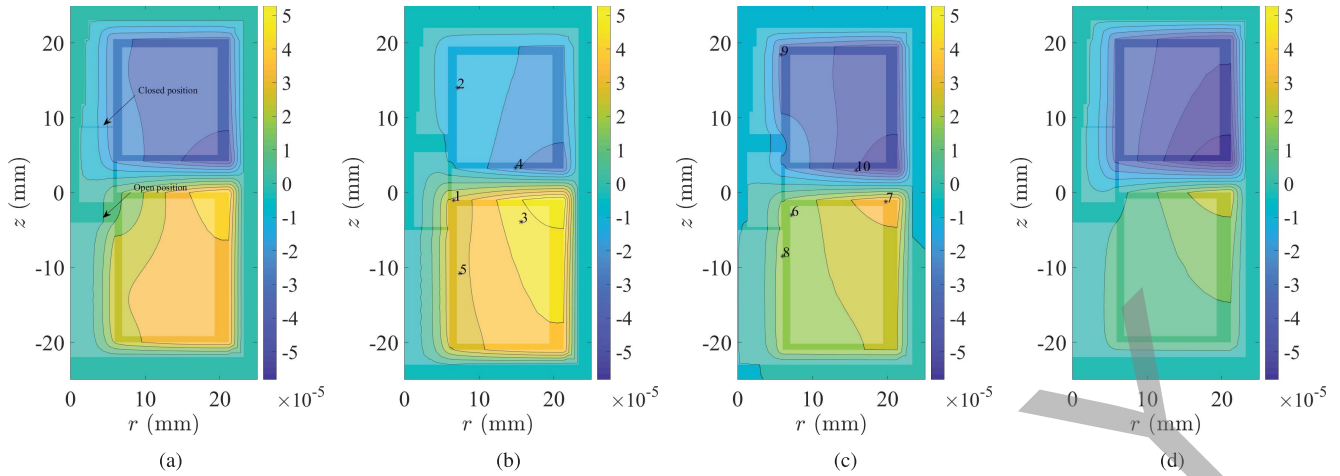


Fig. 9. Distribution of magnetic potential (Wb/m) during different positions of actuator. (a) Closed position: bottom coil on. (b) Open position: bottom coil on. (c) Open position: top coil on. (d) Closed Position: top coil on.

TABLE III
COMPARISON OF COMPUTATIONAL ERRORS OF MAGNETIC FLUX DENSITY (T) AMONG COMSOL, N-R, AND BB-TLM

No.	r/mm	z/mm	COMSOL (T)	N-R (T)	err_3^1	BB-TLM (T)	err_4^2
1	4.246	7.938	0.5200	0.5047	2.95%	0.5114	1.65%
2	14.432	0.118	1.0895	1.0936	0.37%	1.0924	0.26%
3	6.272	13.486	0.0416	0.0423	1.63%	0.0397	4.56%
4	16.429	-3.115	0.1317	0.1331	1.07%	0.1310	0.54%
5	21.967	-16.918	0.7196	0.7729	7.41%	0.7633	6.07%
6	20.983	-14.495	0.0200	0.0206	2.95%	0.0209	4.33%
7	20.983	-11.65	0.0336	0.0326	2.96%	0.0326	3.08%
8	3.37	2.15	1.12E-4	1.31E-4	16.15%	1.23E-4	9.44%
9	19.55	21.797	0.3001	0.2998	0.10%	0.2989	0.40%
10	3.21	-2.03	3.99E-4	4.22E-4	5.92%	4.28E-4	7.34%

$${}^1err_3 = \left| \frac{N-R - COMSOL}{COMSOL} \right| \times 100\%$$

$${}^2err_4 = \left| \frac{BB-TLM - COMSOL}{COMSOL} \right| \times 100\%$$

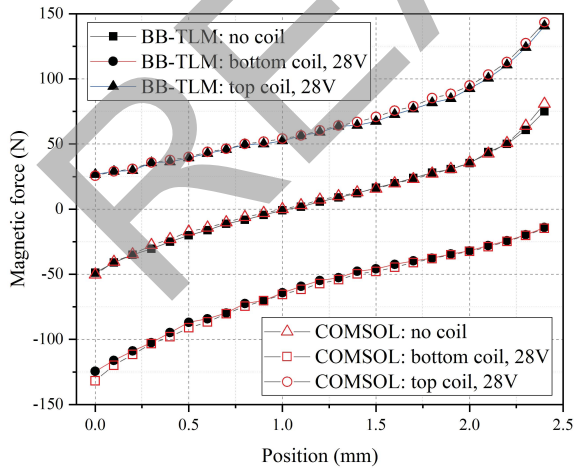


Fig. 10. Comparison of magnetic forces between BB-TLM and COMSOL.

position and closed position is about 2.4 mm in Fig. 9(a) and the moving step of armature is set as 0.1 mm. Those three groups of curves are obtained under three kinds of contactor’s

working conditions: no coil, bottom coil working with 28 V voltage, and top coil working with 28 V voltage. The direction of the force is along the positive direction of z -axis and the armature starts from the open position. Results show there is a close agreement of the force curves between the BB-TLM and COMSOL results and the maximum differences are less than 5% which indirectly shows the results of BB-TLM is correct and acceptable.

E. Convergence Analysis

Generally speaking, the transmission lines inserted into the nonlinear dc network cannot change circuit’s stable status. Thus, after a number of reflections, the voltage of each node will gradually reach steady state. From a physical standpoint, the BB-TLM is unconditionally convergent. To further study the influence factor of the iteration speed, we tested our programs using some numerical experiments to show the influence of some factors, such as the inner iteration error and transmission line’s admittance.

1) *Effect of Inner Iteration Error δ* : When the voltage signals travel toward each nonlinear element, the small nonlinear circuit is solved by N-R iteration. Theoretically, this inner convergence error should be set as small as possible. However, a higher solution precision will bring much more time-consumption. Thus, we tested and analyzed the influence of the inner iteration error. Fig. 11 shows the convergence process under different inner iteration errors when the transmission lines’ admittances keep unchanged. To demonstrate the variation tendency of error, logarithmic coordinates is used. The inner iteration errors δ of curves A, B, C, D, and E are, respectively, $1e-1$, $1e-3$, $1e-6$, $1e-7$, and $1e-10$. When the error is too large, curve A varies fast at the first 100 steps. However, small amplitude oscillation appears in the curve after the 100th step and the solution precision could not be improved. Then, we improve the inner error to $1e-3$, curve B has the same tendency as curve A. Although the oscillation still appears from about 100th step, the precision is obviously enhanced. When the error is set to $1e-6$, the shape of curve C changed distinctly, looking smooth and linear. Curve C is linearly

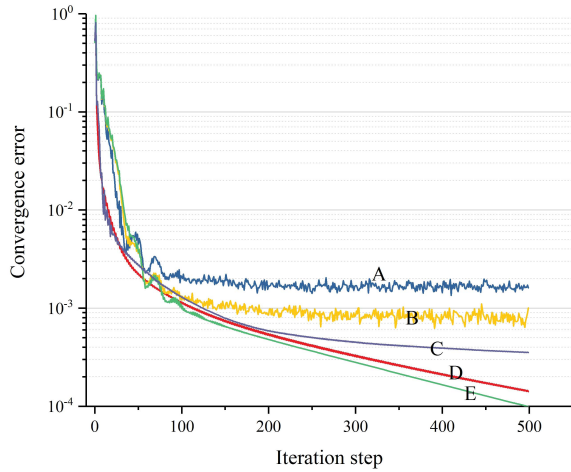


Fig. 11. Convergence process under different inner iteration errors.

convergent and does not show obvious oscillation compared with curves A and B. Curves D and E still have a smooth and linear shape. Unlike curve C, the iteration speed is improved. As discussed earlier, considering the time-consumption, it is a compromise choice to set the inner error δ between $1e-6$ and $1e-7$.

2) *Effect of Transmission Lines' Admittances:* The transmission line's admittance also has a huge impact on the convergence speed of BB-TLM. Different from original two-port circuit component which can use the method of impedance matching to choose a better guess value of admittances, there exists very complex matching relationship in the black-box model. The setting of the admittance is still an open problem. Here, we propose a strategy by setting the corresponding admittance as αK_{ii}^e in each element. Fig. 12 presents different convergence curves by choosing various α (convergence error is $1e-6$). Through numerical experiments, we found that the admittances did have an important influence on the iteration speed. The α values of curves A–F are 1, 2, 4, 5, 8, and 10, respectively. Fig. 12 shows that it obtains relatively faster speed when $\alpha = 1$ and the speed decreases with α increases. Therefore, to accelerate the iterative speed of BB-TLM, we can solve coarse problems and then determine the admittance value by choosing proper αK_{ii}^e .

F. Comparison of Computation Time

Fig. 13 describes the comparison of computation time between traditional N-R method and TLM method proposed in this paper.

The results in Fig. 13(a) show the computation time of one iteration step of model case 10 in Table I using N-R and BB-TLM, respectively, as the computer cores increases. Since the N-R method itself does not have a parallel version, for equitable comparison, a parallel sparse matrix solver SuperLU_MT [31] is adopted to accelerate the iteration. However, Fig. 13(a) shows that the time in single step of N-R method still has a great gap and is more than $20\times$ larger than that of BB-TLM when the number of CPU cores used is 20. For each iteration, BB-TLM only treats those nonlinear

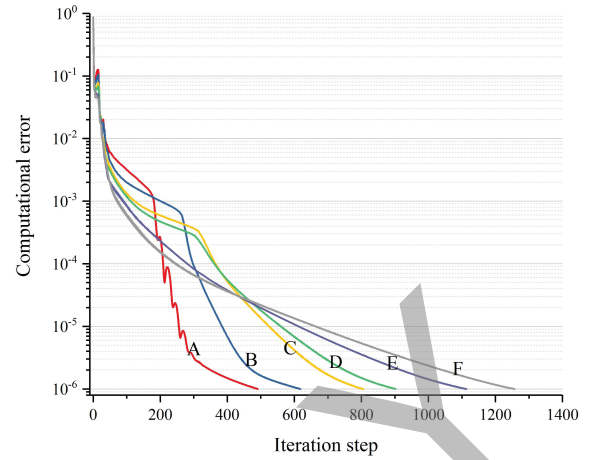


Fig. 12. Effect of the transmission lines' admittances.

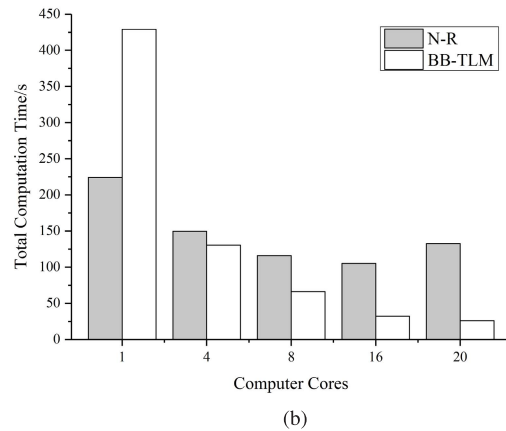
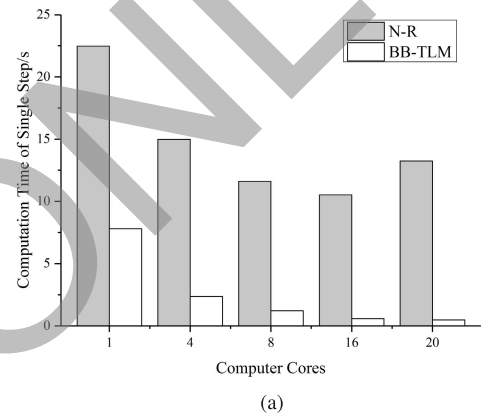


Fig. 13. Comparison of computation time of N-R and BB-TLM. (a) Comparison of single-step time. (b) Comparison of total execution time.

elements which can be run in different cores. With the increase of CPU cores, BB-TLM has obvious acceleration in single-step time.

Fig. 13(b) shows the comparison of total computation time between N-R and BB-TLM. The model used is case 10. Without the parallel computation, BB-TLM runs much slower than N-R which benefits from its fast convergence speed. However, with the increasing of CPU cores, BB-TLM has shown their advantages and it is about five times faster than N-R.

TABLE IV
COMPARISON OF EXECUTION TIMES

Cases	N-R		BB-TLM		Cases	N-R		BB-TLM	
	time/s	steps	time/s	steps		time/s	steps	time/s	steps
1	0.1654	8	0.1506	50	6	15.363	10	7.2826	44
2	0.3213	10	0.2121	50	7	26.135	10	25.3454	51
3	0.6329	9	0.3383	54	8	36.56	10	16.1219	53
4	0.652	10	0.4624	56	9	73.234	10	10.6849	53
5	1.684	10	0.7026	55	10	132.537	10	25.9976	55

TABLE V
COMPARISON OF CALCULATION MODELS WITH ORIGINAL TLM AND BB-TLM

	original TLM		BB-TLM	
	Case 5	Case 10	Case 5	Case 10
Circuit models	6 impedances, 3 current sources	8 impedances, 4 current sources	black-box circuit, no need inside circuit in detail	
Variables per element	6 Y_i , 6 V_r	8 Y_i , 8 V_r	0 Y_i , 3 V_i , 3 V_r	0 Y_i , 4 V_i , 4 V_r
Memory consumption	1492 KB	459 KB	497 KB	153 KB
Nonlinear solution	6 equations	8 equations	3 equations	4 equations

Table IV lists the iteration steps and computation times of both methods with respect to different mesh sizes using 20 CPU cores. Cases 1–5 are the results of triangular shape elements and cases 6–10 are the results of quadrilateral shape elements. Table IV shows that BB-TLM can both deal with the two types of FEM elements and its speedup effect starts to be evident when the mesh size increases. Although BB-TLM’s iteration speed is about five times lower than N-R, it is still faster than the parallelized N-R method, especially in cases 9 and 10. Because in the quadrilateral shape element solution, we used the Gaussian quadrature to obtain the FEM’s coefficient matrix, the solution time is a little longer. We also noticed that the BB-TLM’s time in cases 8 and 9 is less than case 7. It is strange because the mesh size of cases 8 and 9 is greater than case 7. From Table I, it indicates that the number of nonlinear elements of cases 8 and 9 is less. Thus, the computation time of BB-TLM is also affected by the number of nonlinear elements.

G. Comparison With Original TLM

Table V shows the differences of the original TLM and BB-TLM during calculations of cases 5 and 10. The FEM element shapes of cases 5 and 10 are triangular and quadrilateral, respectively. From Table V, we can find that the total components in original TLM’s equivalent circuits increase when the number of element’s nodes increases from 3 to 4. As a result, the size of variables storing the circuit’s information in each element also increases linearly. However, in BB-TLM method, there is no need to build the equivalent circuit model in detail. Thus, the impedances are not need to be stored anymore and the variables of reflection voltages and incidence voltages are less. In each case, the memory consumption of original TLM is

three times larger than BB-TLM’s. What is more, the number of nonlinear equations of original TLM is also two times of BB-TLM’s. Those results show that BB-TLM is easier to model the equivalent circuit and solve the nonlinear problems.

H. Discussion

Overall, this paper has described a parallel BB-TLM method to solve nonlinear finite element problems. Aiming to overcome the TLM’s limitations and constraints in the applications of complex FEM problems, the proposed BB-TLM can be seen as the further development of the original TLM method. By proposing a novel black-box model, each single FEM mesh element can be seen as an independent circuit network. Thus, it not only avoids the complex equivalent circuits model problems existed inside the element but also has a good ability to solve the inside nonlinear coupling relationship using Newton–Raphson iteration.

For the first time, the idea of transmission line iteration can be applied to the solution of FEM problems discretized by quadrilateral shape elements using BB-TLM. The transmission lines inserted in the circuits help to implement the global iteration process of complex elements such as triangular and quadrilateral shape elements, discretize all the nonlinear elements and further fulfill the parallel computation. At the same time, the transmission lines will not change the stable state of the circuit which means this kind of method is always convergent. Results indicate that BB-TLM has the potential in FEM parallel computing. It has a good speedup effect compared with parallelized N-R solver in larger mesh size cases. At present, N-R method is still commonly used for its excellent convergence speed. However, with the increase of mesh size, the dimension of the linear matrix also grows up which bring the time-consumption problems, especially in some repeated computing work. In contrast, BB-TLM includes the solution process of linear regions and nonlinear regions. For linear regions, only the forward and backward substitution processes need to be done if the LU factorization is used which can save more than 95% time. The nonlinear regions can be solved in parallel. There usually exist thousands of nonlinear elements. It will bring a great improvement to the solution time if all the nonlinear jobs can be fully distributed in parallel hardware with thousands of cores such as GPU and high performance computing.

The parallelization and discretization of FEM problems always result in the decrease of the convergence speed. Although we improve the ability of TLM in building complex equivalent circuits, compared with Newton–Raphson method, the iteration speed of BB-TLM is much slower which is affected by the transmission lines’ admittances. By numerical experiments, we pointed out a practical scheme to obtain a suitable admittance’s guess value. However, it still needs to be further studied to understand its exact influence.

In the future, it is also possible to apply this method for transient analysis of electromagnetic devices in which the solution time using FEM is usually very long. It can also be used to other aspects, such as the solution of 3-D FEM problems or other physics fields. More interestingly,

the BB-TLM may be developed as a new kind of domain decomposition method if the solution domain is divided into several nonoverlapping regions which can be seeded as huge elements.

V. CONCLUSION

This paper has proposed a generalized BB-TLM iteration method for finite element simulation of nonlinear axisymmetrical magnetostatic field. A novel black-box equivalent circuit of FEM equation and parallel BB-TLM iteration process are introduced. The black-box model not only greatly reduces the complexity of equivalent circuit network but also enhances the practicability of the original TLM method. Results of magnetic field and magnetic forces have been obtained by the proposed method, which show an excellent agreement with both results of N-R and COMSOL. Moreover, we have presented its acceleration performance with the scheme of parallel process. The BB-TLM has better parallel performance than the conventional Newton–Raphson solver. In the future, we may further study the application of BB-TLM in transient simulation of actuator taking into account movement and electric circuit.

ACKNOWLEDGMENT

This work was supported by the National Natural Science Foundation of China under Grant 51507033.

REFERENCES

- [1] D. D. Giannacopoulos and D. Q. Ren, “Analysis and design of parallel 3-D mesh refinement dynamic load balancing algorithms for finite element electromagnetics with tetrahedra,” *IEEE Trans. Magn.*, vol. 42, no. 4, pp. 1235–1238, Apr. 2006.
- [2] D. Q. Ren and D. D. Giannacopoulos, “Parallel mesh refinement for 3-D finite element electromagnetics with tetrahedra: Strategies for optimizing system communication,” *IEEE Trans. Magn.*, vol. 42, no. 4, pp. 1251–1254, Apr. 2006.
- [3] D. Q. Ren, T. Park, B. Mirican, S. McFee, and D. D. Giannacopoulos, “A methodology for performance modeling and simulation validation of parallel 3-D finite element mesh refinement with tetrahedra,” *IEEE Trans. Magn.*, vol. 44, no. 6, pp. 1406–1409, Jun. 2008.
- [4] G. R. Markall, A. Slemmer, D. A. Ham, P. H. J. Kelly, C. D. Cantwell, and S. J. Sherwin, “Finite element assembly strategies on multi-core and many-core architectures,” *Int. J. Numer. Methods Fluids*, vol. 71, no. 1, pp. 80–97, 2013.
- [5] C. Cecka, A. J. Lew, and E. Darve, “Assembly of finite element methods on graphics processors,” *Int. J. Numer. Methods Eng.*, vol. 85, no. 5, pp. 640–669, 2011.
- [6] K. Ljungkvist, “Finite element computations on multicore and graphics processors,” Ph.D. dissertation, Dept. Inf. Technol., Univ. Uppsala, Uppsala, Sweden, 2017.
- [7] I. Kiss, S. Gyimothy, Z. Badiacs, and J. Pavo, “Parallel realization of the element-by-element FEM technique by CUDA,” *IEEE Trans. Magn.*, vol. 48, no. 2, pp. 507–510, Feb. 2012.
- [8] P. Liu and V. Dinavahi, “Matrix-free nodal domain decomposition with relaxation for massively parallel finite-element computation of EM apparatus,” *IEEE Trans. Magn.*, vol. 54, no. 9, Sep. 2018, Art. no. 7402507.
- [9] C. A. Magele, K. Preis, and W. Renhart, “Some improvements in nonlinear 3D magnetostatics,” *IEEE Trans. Magn.*, vol. 26, no. 2, pp. 375–378, Mar. 1990.
- [10] T. Nakata, N. Takahashi, K. Fujiwara, N. Okamoto, and K. Muramatsu, “Improvements of convergence characteristics of Newton-Raphson method for nonlinear magnetic field analysis,” *IEEE Trans. Magn.*, vol. 28, no. 2, pp. 1048–1051, Mar. 1992.
- [11] S. R. H. Hoole and G. Mahinthakumar, “Parallelism in interactive operations in finite-element simulation,” *IEEE Trans. Magn.*, vol. 26, no. 4, pp. 1252–1255, Jul. 1990.
- [12] V. Rischmuller, M. Haas, S. Kurz, and W. M. Rucker, “3D transient analysis of electromechanical devices using parallel BEM coupled to FEM,” *IEEE Trans. Magn.*, vol. 36, no. 4, pp. 1360–1363, Jul. 2000.
- [13] S. Boehmer, T. Cramer, M. Hafner, E. Lange, C. Bischof, and K. Hameyer, “Numerical simulation of electrical machines by means of a hybrid parallelisation using MPI and OpenMP for finite-element method,” *IET Sci., Meas. Technol.*, vol. 6, no. 5, pp. 339–343, Sep. 2012.
- [14] P. Amestoy *et al.*, “Shared-memory parallelism and low-rank approximation techniques applied to direct solvers in FEM simulation,” *IEEE Trans. Magn.*, vol. 50, no. 2, Feb. 2014, Art. no. 7012704.
- [15] H. W. Dommel, “Digital computer solution of electromagnetic transients in single-and multiphase networks,” *IEEE Trans. Power App. Syst.*, vol. PAS-88, no. 4, pp. 388–399, Apr. 1969.
- [16] P. B. Johns and M. O’Brien, “Use of the transmission-line modelling (t.l.m.) method to solve non-linear lumped networks,” *Radio Electron. Engineer*, vol. 50, no. 1.2, pp. 59–70, Jan./Feb. 1980.
- [17] S. Y. R. Hui and C. Christopoulos, “Numerical simulation of power circuits using transmission-line modelling,” *IEE Proc. A-Phys. Sci., Meas. Instrum., Manage. Educ.*, vol. 137, no. 6, pp. 379–384, Nov. 1990.
- [18] J. Lobry, J. Trecat, and C. Broche, “The transmission line modeling (TLM) method as a new iterative technique in nonlinear 2-D magneto-statics,” *IEEE Trans. Magn.*, vol. 32, no. 2, pp. 559–566, Mar. 1996.
- [19] A. M. Knight, “Time-stepped eddy-current analysis of induction machines with transmission line modeling and domain decomposition,” *IEEE Trans. Magn.*, vol. 39, no. 4, pp. 2030–2035, Jul. 2003.
- [20] O. Deblecker, J. Lobry, and C. Broche, “Use of transmission-line modelling method in FEM for solution of nonlinear eddy-current problems,” *IEE Proc.-Sci., Meas. Technol.*, vol. 145, no. 1, pp. 31–38, Jan. 1998.
- [21] A. M. Knight, “Efficient parallel solution of time-stepped multislice eddy-current induction motor models,” *IEEE Trans. Magn.*, vol. 40, no. 2, pp. 1282–1285, Mar. 2004.
- [22] B. Asghari and V. Dinavahi, “Novel transmission line modeling method for nonlinear permeance network based simulation of induction machines,” *IEEE Trans. Magn.*, vol. 47, no. 8, pp. 2100–2108, Aug. 2011.
- [23] B. Asghari and V. Dinavahi, “Real-time nonlinear transient simulation based on optimized transmission line modeling,” *IEEE Trans. Power Syst.*, vol. 26, no. 2, pp. 699–709, May 2011.
- [24] W. Yang, F. Peng, and V. Dinavahi, “Nonlinear axisymmetric magnetostatic analysis for electromagnetic device using TLM-based finite-element method,” *IEEE Trans. Magn.*, vol. 53, no. 4, Apr. 2017, Art. no. 8000509.
- [25] A. C. Polycarpou, *Introduction to the Finite Element Method in Electromagnetics*. San Rafael, CA, USA: Morgan & Claypool, 2006.
- [26] C. R. Paul, *Analysis of Multiconductor Transmission Lines*. Hoboken, NJ, USA: Wiley, 2008.
- [27] B. Jandaghi and V. Dinavahi, “Real-time FEM computation of nonlinear magnetodynamics of moving structures on FPGA for HIL emulation,” *IEEE Trans. Ind. Electron.*, vol. 65, no. 10, pp. 7709–7718, Oct. 2018.
- [28] P. Liu and V. Dinavahi, “Real-time finite-element simulation of electromagnetic transients of transformer on FPGA,” *IEEE Trans. Power Del.*, vol. 33, no. 4, pp. 1991–2001, Aug. 2018.
- [29] J. Coulomb, “A methodology for the determination of global electro-mechanical quantities from a finite element analysis and its application to the evaluation of magnetic forces, torques and stiffness,” *IEEE Trans. Magn.*, vol. MAG-19, no. 6, pp. 2514–2519, Nov. 1983.
- [30] J. Coulomb and G. Meunier, “Finite element implementation of virtual work principle for magnetic or electric force and torque computation,” *IEEE Trans. Magn.*, vol. MAG-20, no. 5, pp. 1894–1896, Sep. 1984.
- [31] X. Li, J. Demmel, J. Gilbert, I. Grigori, M. Shao, and I. Yamazaki, “SuperLU users, guide,” Lawrence Berkeley Nat. Lab., Univ. California, Berkeley, Berkeley, CA, USA, Tech. Rep. LBNL-44289, Aug. 2011. [Online]. Available: <http://crd.lbl.gov/~xiaoye/SuperLU/>